http://dx.doi.org/10.5012/bkcs.2012.33.9.2861

# Comparison of Different Theory Models and Basis Sets in Calculations of TPOP24N-Oxide Geometry and Geometries of *meso*-Tetraphenyl Chlorin *N*-Oxide Regioisomers

**Sang Joon Choe**

*Department of Chemistry, Institute of Basic Science, Inje University, Kimhae 621-749, Korea. E-mail: chemcsj@inje.ac.kr*
*Received March 10, 2012, Accepted May 24, 2012*

Results of the comparisons of various density functional theory (DFT) methods with different basis sets for predicting the molecular geometry of TPOP24N-Oxide macrocycle, an oxoporphyrin *N*-oxide, are reported in this paper. DFT methods, including M06-2X, B3LYP, LSDA, B3PW91, PBEPBE, and BPV86, are examined. Different basis sets, such as 6-31G*, 6-31+G (d, p), 6-311+G (d, p), and 6-311++G (d, p), are also considered. The M06-2X/6-31G* level is superior to all other density functional methods used in predicting the geometry of TPOP24N-Oxide. The geometries of regioisomeric chlorin *N*-oxide and oxoporphyrin *N*-oxide are reported using M06-2X/6-31G* method. The geometry effects of oxoporphyrin and chlorin *N*-oxide regioisomers are increased β-β bond lengths by *N*-oxidation because the bond overlap index due to charge transfers is decreased. In *N*-oxidation ring (II, III), angles that include β-β bond length increase as the bond overlap index of β-β bond is decreased by *N*-oxidation. The potential energy surfaces of chlorin *N*-oxide and oxoporphyrin *N*-oxide are explored by M06-2X/6-31G*, and single-point calculations are performed at levels up to M06-2X/6-311++G (d, p). Total and relative energies are then calculated. The results indicate that chlorin 24 *N*-oxides are more stable than chlorin 22 *N*-oxides in chlorin *N*-oxide regioisomers. Moreover, TPOP24N-Oxide is less stable than TPOP22N-Oxide.

**Key Words :** Geometry effects, Chlorin *N*-oxide, Oxoporphyrin *N*-oxide regioisomers, DFT

## Introduction

Octaethylporphyrin *N*-oxides, *meso*-tetraarylporphyrin *N*-oxides, and their metal complexes were discovered about 30 years ago.[1-4] The biological significance of these compounds is derived from the presumed involvement of porphyrin *N*-oxide Fe(III) complexes in heme degradation and P-450 suicide reaction.[2,5-7] Their photophysical properties can largely be attributed to their nonplanar conformation and significant structural difference compared with free-base porphyrins. Investigation of porphyrinoid *N*-oxides may yield chromophores with photophysical properties that are more suitable for a given technical or biomedical application than the parent chromophore.[8]

Bruckner *et al*.[8] recently reported the synthesis of two regioisomeric chlorin *N*-oxides and the X-ray structure of *meso*-tetraphenyl-2-oxa-3-oxoporphyrin 24-*N*-oxide (TPOP24N-Oxide).

In the present work, density functional theory (DFT) calculations were performed to elucidate the molecular geometries of TPOP24N-Oxide and two regioisomeric chlorin *N*-oxides. DFT has been extensively used to study various aspects of the porphyrin macrocycle.[9(a)-17] Choe *et al*.[17] reported the geometry of methyl pheophorbide-a and compared the validity of M06-2X with two other functional calculations, namely, B3LYP and LSDA.

The main problem with DFT calculations is that the exact functionals for exchange and correlation are unknown, except for free electron gases. However, approximations in DFT permit the calculation of certain physical quantities quite accurately. The most widely used approximation in physics is the local-density approximation (LDA). Local spin-density approximation (LSDA) is a straightforward generalization of LDA that includes electron spin. The exchange energy in DFT hybrid methods (*e.g.*, M06-2X, B3LYP, B3PW91, PBEPBE, B3PV86) is combined with the exact energy from Hartree–Fock theory. Adjustable parameters in hybrid functional are generally fitted to a training set of molecules. However, although the results obtained from these functionals are usually sufficiently accurate for most applications, no systematic way of improving them has yet been found, in contrast to some traditional wave function-based methods, such as configuration interaction or coupled cluster theory. Hence, estimation of the error of the calculation for the geometry and properties of TPOP24N-Oxide compared with other methods or experiments is necessary.

Thus far, no attempt has been made to analyze the application of various DFT methods and different basis sets for accurate calculations of porphyrin macrocycles and tetraphenyl porpyrin *N*-oxide geometries.

This work has two purposes as follows: (1) to investigate the performance of different DFT methods and the effect of different basis sets in predicting the geometry of TPOP24N-Oxide and (2) to study the geometries of two regioisomeric *meso*-tetraphenyl chlorin *N*-oxides and oxoporphyrin *N*-

oxides, specifically, *meso*-tetraphenyl-2,3-*cis*-dihydroxychlorin 24-*N*-oxide (TPDHC24N-Oxide), *meso*-tetraphenyl-2,3-*cis*-dihydroxychlorin 22-*N*-oxide (TPDHC22N-Oxide), *meso*-tetraphenyl-2,3-dioxochlorin 24-*N*-oxide (TPDOC24N-Oxide), *meso*-tetraphenyl-2,3-dioxochlorin 22-*N*-oxide (TPDOC22N-Oxide), and *meso*-tetraphenyl-2-oxa-3-oxoporphyrin 22-*N*-oxide (TPOP22N-Oxide). Calculated geometries are analyzed by normal-coordinate structural decomposition (NSD).[9,15-17] This study provides a wealth of theoretical data and gives insights into the geometric preferences of TPOPN-Oxide and chlorin *N*-oxide regioisomers.

## Computational Methods

All DFT calculations were carried out using the *Gaussian 09* program.[18] TPOP24N-Oxide geometries were determined through the application of various DFT methods, including M,06-2X, B3LYP, LSDA, B3PW91, PBEPBE, and B3PV86, and different basis sets, including 6-31G*, 6-31+G(d, p), 6-311+G(d, p), and 6-311++G(d, p). TPOP22N-Oxide, TPDHC24N-Oxide, TPDHC22N-Oxide, TPDOC24N-Oxide, and TPDOC22N-Oxide geometries were optimized by M06-2X/6-31G* method. Single-point calculations with a larger basis set, 6-311++G(d, p), were also performed. This basis set describes each valence atomic orbital with three basis functions and contains polarization functions on all atoms.

The bond overlap index and the atomic charges of the TPOP24N-Oxide and the TPOP22N-Oxide were calculated at M06-2X/6-31G* level of theory using the natural bond orbital (NBO)[19-22] method implemented in *Gaussian 09* package.[18] The wiberg bond index[21] obtained by the sums of squares of off-diagonal density matrix element as bond order can be used as a measure of a bond overlap.

M06-2X/6-31G*-optimized geometries were analyzed using NSD.[9,15-17] This method characterizes the chlorin conformation in terms of equivalent displacements along the normal coordinates of the chlorin macrocycle. Typically, the largest static distortions of the chlorin macrocycle occur along the softest normal modes; hence, the greatest contributors to the nonplanar distortion are the lowest-frequency normal coordinates of each out-of-plane symmetry type (*i.e.*, $B_{1u}$, $B_{2u}$, $A_{2u}$, $E_g$, and $A_{1u}$). These deformations correspond to symmetric distortions commonly observed in a structure, and are called ruffling (ruf), saddling (sad), doming (dom), waving (wav(x,y)), and propelling (pro).[9,15-17] They also provide asymmetric macrocyclic distortions of various types, aside from projections of the total distortions when mixed together. Only these six normal coordinates typically, reasonably, and accurately simulate the actual out-of-plane distortion. The *Gaussian 09* and NSD programs on a Silicon Graphics Computer System were used to perform calculations and search for optimum geometries.

## Results and Discussion

### Geometry Optimization with Various Methods Using the 6-31G* Basis Set in the Calculations of TPOP24N-Oxide.

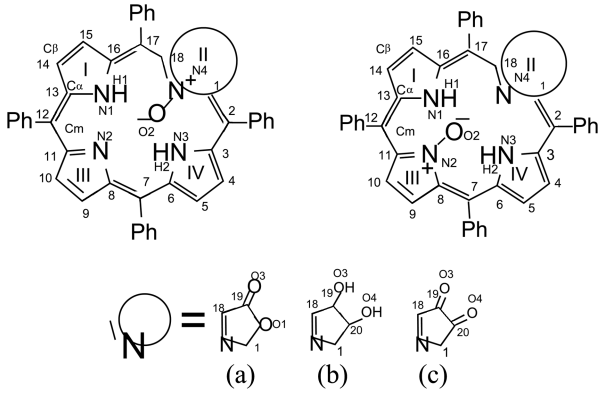


**Figure 1.** Selected geometries to number labels in oxoporphyrin *N*-oxide regioisomer and chlorin *N*-oxide. α-angles are C18-N4-C1 and C11-N2-C8. (a) TPOP24N-Oxide and TPOP22N-Oxide; (b) TPDHC24N-Oxide and TPDHC22N-Oxide; (c) TPDOC24N-Oxide and TPDOC22N-Oxide.

A selected geometry of the TPOP24N-Oxide macrocycle with numerical labels is shown in Figure 1. A comparison of selected bond lengths calculated with various DFT methods using the 6-31G* basis set for the molecular cluster of TPOP24N-oxide is shown in Table S1 of Supporting Information. The results obtained from various DFT calculations using the 6-31G* basis set were compared with experimental results. O1-C19 bond distances yielded by B3LYP, LSDA, B3PW91, PBEPBE, and B3PV86 are significantly overestimated, whereas those calculated using the M06-2X method (1.391 Å) are nearest the values of experimental data. Furthermore, M06-2X predicts C4-C5 (1.368 Å), C6-C7 (1.401 Å), C9-C10 (1.349 Å), C12-C13 (1.402 Å), C14-C15 (1.366 Å), and N4-C1 (1.360 Å) lengths in better agreement with experimental data than all other methods used. The mean absolute deviations between the calculated and experimental values for each method are given in Table 1 to investigate the performance and limits of the different DFT methods in predicting the bond length of TPOP24N-Oxide. Mean absolute deviations between calculated bond lengths and experimental values are 0.006 Å for M06-2X, 0.008 Å for B3LYP, 0.007 Å for LSDA, 0.007 Å for B3PW91, 0.014 Å for PBEPBE, and 0.007 Å for B3PV86. These results indicate that of all the methods tested, M06-2X method is the most suitable for predicting the bond length of TPOP24N-Oxide.

The calculated bond angles of the TPOP24N-Oxide macrocycle obtained using various DFT methods with the 6-31G* basis set are listed in Table S2 of Supporting Information.

Mean absolute deviations between the calculated bond angles and experimental values are 0.692° for M06-2X, 0.640° for B3LYP, 0.813° for LSDA, 0.679° for B3PW91, 0.711° for PBEPBE, and 0.690° for B3PV86. These values are listed in Table 1. The results indicate that mean absolute deviations obtained from B3LYP are the smallest among the various methods used. To investigate the geometry of porphyrinoid compounds, many researchers[9-17] have studied the geometry of porphyrin macrocycle and chlorin because of

**Table 1.** Comparison of mean absolute deviations calculated with various DFT methods using the 6-31G* basis set for the molecular cluster model of TPOP24N-Oxide macrocycle

| | M06-2X | B3LYP | LSDA | B3PW91 | PBEPBE | B3PV86 |
|---|---|---|---|---|---|---|
| Lengths | 0.006 | 0.008 | 0.007 | 0.007 | 0.014 | 0.007 |
| Percentage[a] (A%) | 0.446 | 0.625 | 0.521 | 0.521 | 1.343 | 0.521 |
| Angles | 0.692 | 0.640 | 0.813 | 0.679 | 0.711 | 0.690 |
| Percentage[b] (B%) | 0.589 | 0.544 | 0.692 | 0.577 | 0.605 | 0.589 |
| Mean Percentage[c] (C%) | 0.518 | 0.585 | 0.607 | 0.549 | 0.974 | 0.555 |

[a] $\frac{\text{Mean absolute deviations of bond length}}{\text{Mean bond lengths of experimental value}} \times 100 = \text{A\%}$ . [b] $\frac{\text{Mean absolute deviations of bond angle}}{\text{Mean bond angles of experimental value}} \times 100 = \text{B\%}$ · [c] $\frac{\text{A\%+B\%}}{2} = \text{C\%}$

biological significance.

Mean percentages are defined as the mean value of a sum of error percentage for the mean absolute deviations of bond length and for the bond angles. The calculated mean percentages are listed in Table 1. For the bond, length deviations and bond angle are the most meaningful in the selected geometry of the TPOP24N-Oxide macrocycle. The mean percentages are 0.518% for M06-2X, 0.585% for B3LYP, 0.607% for LSDA, 0.549% for B3PW91, 0.974% for PBEPBE, and 0.555% for B3PV86, respectively. The results indicate that of all the methods tested, M06-2X is the most suitable for predicting the geometry in Table 1.

In Table S3 of Supporting Information, root-mean square deviations (RMSD) between x-ray structure coordinates of the TPOP24N-Oxide macrocycle and calculated structure coordinates are 0.182 Å for M06-2X, 0.159 Å for B3LYP, 0.155 Å for LSDA, 0168 Å for B3PW91, 0.251 Å for PBEPBE, and 0.149 Å for B3PV86, respectively. The results indicate that RMSD obtained from B3PV86 is the most suitable for predicting the structure of TPOP24N-Oxide. However, M06-2X method was selected for further calculations because our main purpose in this paper was to investigate the geometries.

Calculated N4-C18-C17, C2-C3-C4, and H1-N1-C13 angles of TPOP24N-Oxide obtained using various DFT methods with the 6-31G* basis set are smaller than the experimental values by about 1.6° to 2.6°, whereas the calculated N1-C16-C17 angle increases by 1.1° to 1.4° compared with the experimental data. Other calculated angles for TPOP24N-Oxide using various DFT methods with the 6-31G* basis set are very close to experimental values.[8] In this paper, dihedral angles are fixed for calculating TPOP24N-Oxide geometries.

**Geometry Optimization Using M06-2X Method with Various Bases Sets in TPOP24N-Oxide Calculations.** The effects of different basis sets on the geometry of TPOP24N-Oxide are calculated using M06-2X method. A comparison of selected bond lengths and angles of the TPOP24N-oxide macrocycle is presented in Tables S4 and S5 of Supporting Information.

Table S6 of Supporting Information shows that mean absolute deviations between calculated bond lengths and experimental values are 0.006 Å for 6-31G*, 0.006 Å for 6-31+G (d, p), 0.007 Å for 6-311+G (d, p), and 0.007 Å for 6-311++G (d, p). Mean deviations of the 6-31G* basis set equal those of 6-31+G (d, p), at 0.006 Å, whereas mean deviations of the 6-311+G (d, p) basis set are identical to those of 6-311++G (d, p) at 0.007 Å. Mean absolute deviations between calculated bond angles and experimental values are 0.692° for 6-31G*, 0.697° for 6-31+G (d, p), 0.692° for 6-311+G (d, p), and 0.692° for 6-311++G (d, p). Mean deviations from 6-311+G (d, p) are equal to those from 6-311++G (d, p), indicating that the 6-31G* basis set is the most suitable for predicting the geometry of TPOP24N-Oxide.

With the 6-31G* basis set, the maximum absolute deviation of bond length at O2-N4 is 0.046 Å. Calculated C6-C7, C12-C13, and N3-C3 lengths of TPOP24N-Oxide are very close to the experimental values.[8] The maximum angle is 2.1° at C2-C3-C4, whereas the minimum angle is 0° at O2-N4-C1. Calculated C1-C2-C3, C10-C11-C12, and C18-C19-O3 angles are very close to the experimental values.[8]

**Geometry Effects of Oxoporphyrin and Chlorin *N*-Oxide Regioisomers.** The effects of regioisomers on the geometry of oxoporphyrin *N*-oxides and chlorin *N*-oxides were investigated using M06-2X method. The 6-31G* basis set is the most suitable for predicting the geometry of TPOP24N-Oxide, so its application was extended to chlorin *N*-oxides. Bond distances and angles of TPOP22N-Oxide and chlorin *N*-oxides calculated using M06-2X method with 6-31G* are presented in Tables S7 and S8 of Supporting Information. In oxoporphyrin *N*-oxide regioisomers (*i.e.*, TPOP24N-Oxide and TPOP22N-Oxide), the bond distance of C18-C19 is 1.474 Å for TPOP24N-Oxide and 1.495 Å for TPOP22N-Oxide. The bond distance of O1-C19 decreases by 0.013 Å in TPOP22N-Oxide compared with TPOP24N-Oxide; by contrast, the N2-C11 of TPOP22N-Oxide increases by 0.030 Å.

C18-C19-O1 angle and C19-O1-C1 of TPOP22N-Oxide decrease by 1.7° compared with TPOP24N-Oxide. C19-O1-C1 angle is 109.0° for TPOP24N-Oxide and 107.3° for TPOP22N-Oxide. In ring III, C11-C10-C9 and C10-C9-C8 angles are 106.2° and 106.1° for TPOP24N-Oxide and 107.9° and 108.0° for TPOP22N-Oxide, respectively.

Table 2 shows selected atomic charges of the regioisomers by *N*-oxidation in oxoporphyrin *N*-oxides and chlorin *N*-oxides. The atomic charge of C18 and C19 of C18-C19 bond are 0.020 and 0.803 for TPOP24N-Oxide and 0.057 and 0.799 for TPOP22N-Oxide. For O1-C19 bond, atomic charges of O1 and C19 are –0.527 and 0.803 for TPOP24-Oxide, and

–0.538 and 0.799 for TPOP22N-Oxide. For N2-C11bond, N2 charges are –0.553 for TPOP24N-Oxide and 0.045 for TPOP22N-Oxide. C11 charges are 0.170 and 0.111. These results indicate the atomic charge transfers by *N*-oxidation.

In Table 3, the bond overlap index of C18-C19 bond, O1-C19, and N2-C11 is 1.040, 0.904, and 1.325, respectively, for TPOP24N-Oxide. For TPOP22N-Oxide, the bond overlap index is 1.003 for C18-C19 bond, 0.925 for O1-C19, and 1.108 for N2-C11, respectively. The changes of bond length are attributed to the bond overlap index due to charge transfers. Thus, the bond overlap index becomes bigger as the bond length decreases.

In the case of *N*-oxidation of ring II, β-β bond length (C19-O1) of TPOP24N-Oxide is larger than that of TPOP22N-Oxide because the bond overlap index of O1-C19 bond for TPOP24N-Oxide is smaller than that of TPOP22N-Oxide. In ring III *N*-oxidation, β-β bond length (C9-C10) of TPOP22N-Oxide is larger than that of TPOP24N-Oxide because the bond overlap index of C10-C9 bond for TPOP22N-Oxide is smaller than that of TPOP24N-Oxide. Therefore, β-β bond lengths are increased by *N*-oxidation; by contrast, the bond overlap index is decreased. Angles that include β-β bond lengths, specifically, C18-C19-O1, C19-O1-C1, C11-C10-C9, and C10-C9-C8 in rings II and III, are also increased by N-oxidation, as the bond overlap index of β-β bond length decreases.

In dihydroxychlorin *N*-oxide regioisomers (*i.e.*, TPDHC24N-Oxide and TPDHC22N-Oxide), C18-C19 bond length of TPDHC24N-Oxide is 1.507 Å, whereas that of TPDHC22N-Oxide is 1.520 Å. C20-C19 bond length and C9-C10 of TPDHC24N-Oxide are 1.543 and 1.351 Å, respectively; those for TPDHC22N-Oxide are 1.529 and 1.359 Å, respectively.

For TPDHC24N-Oxide, bond angles of C18-C19-C20, C19-C20-C1, C11-C10-C9, and C10-C9-C8 are 102.9°, 102.8°, 106.1°, and 106.1°, respectively; those corresponding to TPDHC22N-Oxide are 101.2°, 101.6°, 108.0°, and 107.9°, respectively.

In Table 2, the atomic charges of C18 and C19 in C18-C19 bond are 0.179 and 0.067 for TPDHC24N-Oxide, and 0.225 and 0.050 for TPDHC22N-Oxide. For C20-C19 bond, the atomic charges of C20 and C19 are 0.052 and 0.067 for TPDH C24N-Oxide, and 0.034 and 0.050 for TPDHC22N-Oxide. For C10-C9, the atomic charges of C10 and C9 are –0.271 and –0.261 for TPDHC24N-Oxide, and –0.477 and –0.267 for TPDHC22N-Oxide. These results indicate atomic charge transfers by *N*-oxidation. C20-C19 bond length of TPDHC24N-Oxide is larger than that of TPDHC22N-Oxide because the overlap index due to charge transfers of TPDHC24N-Oxide is smaller than that of TPDHC22N-Oxide. The bond length of C10-C9 is increased by *N*-oxidation because the overlap index of TPDHC22N-Oxide is smaller than that of TPDHC24N-Oxide, as shown in Table 3. The C18-C19 bond length of TPDHC24N-Oxide is smaller than that of TPDHC22N-Oxide because the overlap index of C18-C19 of TPDHC24N-Oxide is larger than that of TPDHC22N-Oxide.

In dioxochlorin *N*-oxide regioisomers (*i.e.*, TPDOC24N-Oxide and TPDOC22N-Oxide), C18-C19 bond distance of TPDOC24N-Oxide and TPDOC22N-Oxide are 1.478 and 1.498 Å, respectively. Bond distance of TPDOC24N-Oxide at C19-C20 and C9-C10 are 1.540 and 1.348 Å, respectively; those corresponding to TPDOC22N-Oxide are 1.533 and 1.356 Å, respectively.

For TPDOC24N-Oxide, the bond angles of C18-C19-C20,

**Table 2.** Selected atomic charges[a] of the regioisomers by *N*-oxidation in oxoporphyrin *N*-oxide macrocycle and chlorin *N*-oxides

| | TPOP24N -Oxide | TPOP22N -Oxide | TPDHC24N -Oxide | TPDHC22N -Oxide | TPDOC24N -Oxide | TPDOC22N -Oxide |
|---|---|---|---|---|---|---|
| C9 | –0.261 | –0.262 | –0.261 | –0.267 | –0.257 | –0.259 |
| C10 | –0.261 | –0.254 | –0.271 | –0.477 | –0.260 | –0.255 |
| C11 | 0.170 | 0.111 | 0.168 | 0.108 | 0.178 | 0.118 |
| C18 | 0.020 | 0.057 | 0.179 | 0.225 | 0.036 | 0.085 |
| C19 | 0.803 | 0.799 | 0.067 | 0.050 | 0.466 | 0.467 |
| N2 | –0.553 | 0.045 | –0.553 | 0.047 | –0.569 | 0.042 |
| O1 | –0.527 | –0.538 | – | – | – | – |
| C20 | – | – | 0.052 | 0.034 | 0.467 | 0.468 |

[a]Atomic charges were calculated at the M062X/6-31G* level of theory using the natural bond orbital (NBO) method.[20,22]

**Table 3.** Selected bond overlap index[a] of the regioisomer by *N*-oxidation in oxoporphyrin *N*-oxide macrocycle and chlorin *N*-oxide

| | TPOP24N -Oxide | TPOP22N -Oxide | TPDHC24N -Oxide | TPDHC22N -Oxide | TPDOC24N -Oxide | TPDOC22N -Oxide |
|---|---|---|---|---|---|---|
| O1-C19 | 0.904 | 0.925 | – | – | – | – |
| C20-C19 | – | – | 0.959 | 1.119 | 0.908 | 0.912 |
| C18-C19 | 1.040 | 1.003 | 0.985 | 0.972 | 1.033 | 0.998 |
| C10-C9 | 1.709 | 1.676 | 1.696 | 1.657 | 1.717 | 1.676 |
| C10-C11 | 1.117 | 1.148 | 1.128 | 1.164 | 0.974 | 1.149 |
| N2-C11 | 1.325 | 1.108 | 1.359 | 1.138 | 1.329 | 1.135 |

[a]Bond overlap index was calculated at the M062X/6-31G* level of theory using the natural bond orbital (NBO) method.[20,22]

C19-C20-C1, C11-C10-C9, and C10-C9-C8 are 105.6°, 105.6°, 106.1°, and 106.1°, respectively; the corresponding angles of TPDOC22N-Oxide are 103.8°, 103.9°, 108.0°, and 107.9°, respectively. In all chlorin *N*-oxide and oxoporphyrin *N*-oxide regioisomers, β-β bond lengths and angles of C18-C19-C20, C19-C20-C1, C11-C10-C9, and C10-C9-C8 in rings II and III are also increased by *N*-oxidation.

In Table 2, the atomic charge of C18 and C19 in C18-C19 bond is 0.036 and 0.466 for TPDOC24N-Oxide, and 0.085 and 0.467 for TPDOC22N-Oxide. For C19-C20 bond, the atomic charges of C19 and C20 are 0.466 and 0.467 for TPDOC24N-Oxide, and 0.467 and 0.468 for TPDOC22N-Oxide. For C10-C9, the atomic charges of C9 and C10 are −0.257 and -0.260 for TPDOC24N-Oxide, and −0.259 and −0.255 for TPDOC22N-Oxide.

In Table 3, the bond overlap indices of C18-C19 bond, C19-C20, and C10-C9 are 1.033, 0.908, and 1.717 for TPDOC24N-Oxide. For TPDOC24N-Oxide, the values are 0.998, 0.912, and 1.676, respectively. Therefore, the changes of C18-C19 bond, C19-C20, and C10-C9 can be attributed to the changes of bond length by the bond overlap index due to charge transfers.

In dihydroxychlorin *N*-oxide regioisomers (*i.e.*, TPDHC24 *N*-Oxide and TPDHC22N-Oxide) and dioxochlorin *N*-oxide (*i.e.*, TPDOC24N-Oxide and TPDOC22N-Oxide), the geometry effects of chlorin *N*-oxide regioisomers are increased β-β bond lengths by *N*-oxidation because the bond overlap index is decreased. In the case of *N*-oxidation of ring II and III, angles that include β-β bond length are also increased because the bond overlap index of β-β bond length is decreased by *N*-oxidation in chlorin *N*-oxide.

In addition, N-O bond lengths in oxoporphyrin and chlorin *N*-oxide are 1.291 Å for TPOP24N-Oxide, 1.302 Å for TPOP22N-Oxide, 1.284 Å for TPDHC24N-Oxide, 1.303 Å for TPDHC22N-Oxide, 1.265 Å TPDOC24N-Oxide, and 1.304 Å for TPDOC22N-Oxide. The N-O bond lengths in oxoporphyrin and chlorin *N*-oxide are longer than normal N-O bonds, such as N-O (1.150 Å) in NO,[23] but are shorter than the N-O bond (1.388 Å) in (CH3)3NO,[24] which has some sigma bond character. A dative N-O bond is usually longer than a normal N-O bond, which explains in part why the N-O bond in oxoporphyrin and chlorine *N*-Oxide has a larger than normal value.[23] Chiang[25] discussed the foregoing phenomenon in pyridine *N*-oxide. He assumed that pyridine-N-Oxide is more aromatic than pyridine itself.[25] The results obtained in this paper are in reasonable agreement with Chiang's discussions. The angles that include β-β bond length and the α-angles are also in consonance with Chiang's discussion. Therefore, the bond angles that include β-β bond length in rings (II and III), as well as the α-angle, increase as the ring (II and III) by N-oxidation increases the aromaticity.

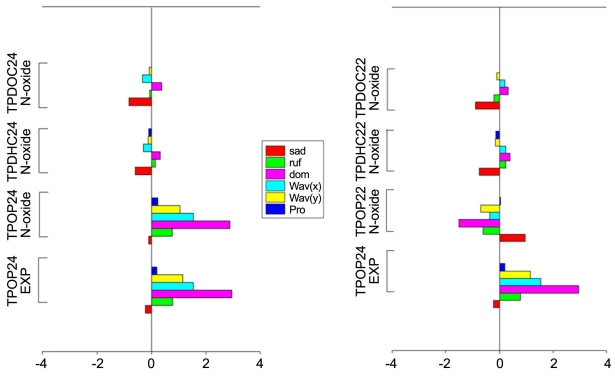


**Figure 2.** Lowest-frequency normal-coordinate structural decomposition results for oxoporphyrin *N*-oxide and chlorin *N*-oxide using M06-2X/6-31G* calculations. Oxoporphyrin *N*-oxides include TPOP24N-Oxide and TPOP22N-Oxide. Chlorin *N*-oxides include TPDHC24N-Oxide, TPDOC24N-Oxide, TPOP22N-Oxide, TPDHC22N-Oxide, and TPDOC22N-Oxide. TPOP24 EXP is the single crystal X-ray structure of TPOP24N-Oxide.

Figure 2 shows the NSD analysis results of the oxoporphyrin *N*-oxides and chlorin *N*-oxides. The calculated TPOP24N-Oxide geometry is in good agreement with TPOP24 EXP, the single crystal X-ray structure of TPOP24N-Oxide.[8] Comparing TPOP24N-Oxide and TPOP22N-Oxide, changes in the out-of-plane deformation are larger in TPOP24N-Oxide. From detailed NSD results of TPOP24N-Oxide shown in Figure 2, saddling is -0.108 Å, ruffling is 0.077 Å, doming is 2.878 Å, Wav(x) is 1.542 Å, Wav(y) is 1.054 Å, and pro is 0.228 Å. In TPOP22N-Oxide, saddling is 0.966 Å, ruffling is −0.613 Å, doming is −1.518 Å, Wav(x) is −0.370 Å, Wav(y) is −0.693 Å, and pro is 0.044 Å. For chlorin *N*-oxide regioisomers, out-of-plane deformations slightly change. The NSD of TPDH24N-Oxide is −0.601 Å for saddling and

**Table 4.** Total and relative energies of regioisomers of oxoporphyrin *N*-oxide and chlorin *N*-oxide

| Molecules | M06-2X/6-31G* | | M06-2X/6-311++G(d,p) | |
|---|---|---|---|---|
| | Total Energy[a] | Erel[b] | Total Energy[a] | Erel[b] |
| TPOP24 *N*-Oxide | −2099.168234 | 0.00 | −2099.705380 | 0.00 |
| TPOP22 *N*-Oxide | −2099.182184 | −8.75 | −2099.718870 | −8.46 |
| TPDHC24 *N*-Oxide | −2139.638409 | 0.00 | −2140.205617 | 0.00 |
| TPDHC22 *N*-Oxide | −2139.635853 | 1.60 | −2140.202555 | 1.92 |
| TPDOC24 *N*-Oxide | −2137.235673 | 0.00 | −2137.783402 | 0.00 |
| TPDOC22 *N*-Oxide | −2137.221522 | 8.88 | −2137.769384 | 8.79 |

[a]Total energies in atomic units. [b]Relative Energies ($E_{rel}$) in Kcal/mol indicate the differences between regioisomers in total energy. Minus sign represents more stable TPOP22N-Oxide thanTPOP24N-Oxide.

0.316Å for doming. TPDH22N-Oxide yields results of −0.751 Å for saddling and 0.392 Å for doming. TPDOC24N-Oxide yields results of −0.826 Å for saddling and 0.372 Å for doming, and TPDOC22 *N*-Oxide yields results of −0.898 Å for saddling and 0.333 for Å doming. These results indicate that macrocycles of oxoporphyrin *N*-oxides obtain larger distortions than chlorin *N*-oxides. Doming deformations are larger in oxoporphyrin *N*-oxides, whereas saddling is larger in chlorin *N*-oxides. The doming of TPOP24N-Oxide is largest among all deformations observed.

Total and relative energies are listed in Table 4. The relative energies, $E_{rel}$, are given in Kcal/mol with respect to stable regioisomers. Minus sign represents the more stable geometry of TPOP22N-Oxide than that of TPOP24N-Oxide. Chlorine 24 *N*-oxide is more stable than chlorine 22 *N*-oxide in chlorin *N*-oxide regioisomers. $E_{rel}$ values of M06-2X/6-31G* and M06-2X/6-311++G (d, p) computed are virtually the same in Table 4. In fact, all $E_{rel}$ values computed with the M06-2X method, using either one of the basis sets and with either one of the optimized geometries, differ by less than 0.32 Kcal/mol.

## Conclusions

The most important findings of this work are the following:

a) The M06-2X/6-31G* level is superior to all other DFT levels used in predicting the geometries of TPOP24*N*-oxide.

The bigger bond overlap index is attributed to the greater bond length decrease by *N*-oxidation.

b) β-β bond lengths increase because bond overlap index is decreased by *N*-oxidation. Angles that include β-β bond length are also increased by *N*-oxidation as the bond overlap of β-β bond length decreases.

c) Chlorin 24 *N*-oxide is more stable than chlorin 22 *N*-oxide in chlorin *N*-oxide regioisomers; TPOP24*N*-oxide is less stable than TPOP22*N*-oxide.

d) NSD shows much smaller macrocyclic distortions in oxoporphyrin *N*-oxide and chlorin *N*-oxide. Oxoporphyrin *N*-oxides exhibit doming distortion, whereas chlorin *N*-oxides exhibit saddling distortion.

## References


1. Bonnett, R.; Ridge, R. J.; Appelman, E. H. *J. Chem. Soc., Chem. Commun*. **1978**, 310-311.
2. Balch, A. L.; Chan, Y. W.; Olmstead, M.; Renner, M. W. *J. Am. Chem. Soc*. **1985**, *107*, 2393-2398.
3. Balch, A. L.; Chan, Y. W.; Olmstead, M. M. *J. Am. Chem. Soc*. **1985**, *107*, 6510-6514.
4. Yang, F. A.; Guo, C. W.; Chen, Y. J.; Chen, J. H.; Wang, S. S.; Tung, J. Y.; Hwang, L. P.; Elango, S. *Inorg. Chem*. **2007**, *46*, 578-585.
5. Mizutani, Y.; Watanabe, Y.; Kitagawa, T. *J. Am. Chem. Soc.* **1994**, *116*, 3439-3441.
6. Rachlewicz, K.; Latos-Grazynski, L. *Inorg. Chem*. **1996**, *35*, 1136-1147.
7. (a) Groves, J. T.; Watanabe, Y. *J. Am. Chem. Soc*. **1986**, *108*, 7836-7837. (b) Groves, J. T.; Watanabe, Y. *J. Am. Chem. Soc*. **1988**, *110*, 8443-8452.
8. Banerjee, S.; Zeller, M.; Bruckner, C. *J. Org. Chem*. **2010**, *75*, 1179-1187.
9. (a) Ghosh, A. In *The Porphyrin Handbook*; Kardish, K. M., Smith, K. M., Guilard, R., Eds.; Academic Press: New York, 2000; Vol. 7, p 1. (b) Shelnutt, J. A. In *The Porphyrin Handbook*; Kardish, K. M., Smith, K. M., Guilard, R., Eds.; Academic Press: New York, 2000; Vol. 7, p 167. (c) Pandey, R. K.; Zheng, G. In *The Porphyrin Handbook*; Kardish, K. M., Smith, K. M., Guilard, R., Eds.; Academic Press: New York, 2000; Vol. 6, p 158.
10. Ghosh, A. *Acc. Chem. Res*. **1998**, *31*, 189-198.
11. Chen, D.-M.; Liu, X.; He, T.-J.; Liu, F.-C. *Chem. Phys. Lett*. **2002**, *361*, 106-114.
12. Sundholm, D. *Phys. Chem. Chem. Phys*. **2000**, *2*, 2275-2281.
13. Parusel, A. B. J.; Wondimagegen, T.; Gosh, A. *J. Am. Chem. Soc*. **2000**, *122*, 6371-6374.
14. Chen, D.-M.; Liu, X.; He, T.-J.; Liu, F.-C. *Chem. Phys.* **2003**, *289*, 397-407.
15. Kim, Na.; Kim, S.; Kim, J. D.; Huh, D. S.; Shim, Y. K.; Choe, S. *J. Bull. Korean Chem. Soc.* **2009**, *30*, 205-213.
16. Kim, N.; Kim, S.; Kim, J. D.; Huh, D. S.; Shim, Y. K.; Choe, S. J. *Bull. Korean Chem. Soc.* **2009**, *30*, 205-213.
17. Huh, D. S.; Choe, S. J. *J. Porphyrins Phthalocyanines* **2010**, *14*, 592-604.
18. Frisch, M. J.; Trucks, G. W.; Schlegel, H. B.; Gill, P. M. W.; Johnson, B. G.; Robb, M. A.; Cheeseman, J. R.; Keith, T.; Peterson, G. A.; Montgometry, J. A.; Raghavacari, K.; Al-Laham, M. A.; Zakrzewski, V. G.; Ortiz, J. V.; Foresman, J. B.; Cioslowski, J.; Stefanov, B. B.; Nanayakkara, A.; Challacombe, M.; Peng, C. J.; Ayala, P. Y.; Chen, W.; Wong, M. W.; Andres, J. L.; Replogle, E. S.; Gomperts, R.; Martin, R. L.; Fox, D. L.; Binkley, J. S.; Defrees, D. J.; Baker, J.; Stewart, J. P.; Head-Gordon, M.; Gonzalez, C.; Pople, J. A. *Gaussian*, Inc.: Wallingford, CT, 2009.
19. Mayer, I. *J. Comput. Chem*. **2007**, *28*, 204-221.
20. Brunck, T. K.; weinhold, F. *J. Am. Chem. Soc*. **1979**, *101*, 1700-1709.
21. Wiberg, K. B. *Tetrahedron* **1968**, *24*, 1083-1096.
22. Feyten, D.; Chaume, G.; Chassaing, G.; Lavielle, S.; Brigaud, T.; Byun, B. J.; Kang, Y. K.; Miclet, E. *J. Phys. Chem. B* **2012**, *116*, 4069-4079.
23. Shaw, J. H. *J. Chem. Phys*. **1956**, *24*, 399-402.
24. Caron, A.; Palenik, G. J.; Goldish, E.; Donohue, J. *Acta Crystallogr.* **1964**, *17*, 102-108.
25. Chiang, J. F. *J. Chem. Phys*. **1974**, *61*, 1280-1283.